

# High-Temperature Oxidation Behavior of Two Nickel-Based Superalloys Produced by Metal Injection Molding for Aero Engine Applications

BENEDIKT ALBERT, RAINER VÖLKL, and UWE GLATZEL

For different high-temperature applications like aero engines or turbochargers, metal injection molding (MIM) of superalloys is an interesting processing alternative. For operation at high temperatures, oxidation behavior of superalloys produced by MIM needs to match the standard of cast or forged material. The oxidation behavior of nickel-based superalloys Inconel 713 and MAR-M247 in the temperature interval from 1073 K to 1373 K (800 °C to 1100 °C) is investigated and compared to cast material. Weight gain is measured discontinuously at different oxidation temperatures and times. Analysis of oxidized samples is done *via* SEM and EDX-measurements. MIM samples exhibit homogeneous oxide layers with a thickness up to 4  $\mu\text{m}$ . After processing by MIM, Inconel 713 exhibits lower weight gain and thinner oxide layers than MAR-M247.

DOI: 10.1007/s11661-014-2391-1

© The Minerals, Metals & Materials Society and ASM International 2014

## I. INTRODUCTION

MATERIALS used in aero engines or stationary gas turbines for electric power production have to withstand demanding conditions. The efficiency of turbines depends on the inlet temperature of the turbine as well as on the tightness of various air seals. The maximum temperature is limited by the materials in the hot gas path of the turbine. Knowledge of the high-temperature behavior and oxidation resistance of the materials used is needed to ensure that no failure occurs.

Nickel-based superalloys used in stationary gas turbines or aero engines are normally produced by casting or powder metallurgy. Since ever growing economic and ecological demands, the desire is to optimize the material either performance-wise or cost-wise. For small parts like nozzles, seals, or vanes, metal injection molding (MIM) has emerged as a rather new possibility for high temperature materials if the no. of required parts is high enough. The metal injection molding process is described extensively in the literature.<sup>[1,2]</sup> For the majority of MIM parts in use nowadays, high-temperature behavior is not an issue. The main targets are cost reductions and good forming possibilities.<sup>[1]</sup>

While MIM of steel parts is well established, injection molded superalloy parts are used rarely up to now. However, there is an increasing no. of studies about injection molding of superalloys.<sup>[3-14]</sup> Mechanical properties of MIM-produced superalloys have been reported,

but there is very little literature data of the oxidation resistance of MIM-produced nickel-based superalloys. It has to be certified that the high-temperature oxidation behavior of these alloys is as good as of conventionally produced cast or forged alloys, so that MIM parts are an alternative to use. In this study, the high-temperature oxidation behavior of nickel-based superalloys Inconel 713 (IN 713) and MAR-M247 (M247) is investigated. The composition of both alloys is shown in Table I.

Both alloys are  $\gamma'$ -forming superalloys with a high vol. content of 60 to 70-vol. pct  $\gamma'$ -precipitates. With an Al-content of 6 pct and a Cr-content of 8 and 12 pct, respectively, (see Table I) both alloys form a protective  $\text{Al}_2\text{O}_3$  layer during oxidation, based on the ternary alloy system Ni-Cr-Al.<sup>[15]</sup> The composition is in a range that both alloys show transient oxidation behavior, meaning faster growing oxides control the oxidation behavior initially before a dense  $\text{Al}_2\text{O}_3$  layer forms. Usually, this results in an oxidation mechanism with three distinct oxide layers.<sup>[15-17]</sup> In ternary alloys, these three are in order from inner to outer oxide layer  $\text{Al}_2\text{O}_3$ , a combination of  $\text{Cr}_2\text{O}_3$  and spinel, and NiO as outer layer. Beneath the  $\text{Al}_2\text{O}_3$ -layer, a depletion of  $\gamma'$ -precipitates occurs. In commercial superalloys with a high no. of alloying elements, different other oxides contribute to these layers, especially in the middle layer.

## II. EXPERIMENTAL

Specimens from nickel-based superalloys IN 713 and MAR-M247 produced by MIM are provided by Schunk Sintermetalltechnik, Thale, Germany. The composition is given in Table I. Sintering parameters for both alloys have been evaluated before by an extensive experimental test program. Parameters used in this study are shown in Table II.

---

BENEDIKT ALBERT, formerly Research Scientist with the Metals and Alloys, University of Bayreuth, Bayreuth, Germany, is now with the MTU Aero Engines, Munich. RAINER VÖLKL, Senior Scientist, and UWE GLATZEL, University Professor, are with the Metals and Alloys, University of Bayreuth. Contact e-mail: uwe.glatzel@uni-bayreuth.de

Manuscript submitted February 16, 2014.

Article published online June 17, 2014

**Table I. Nominal Composition of Ni-Based Superalloys IN 713 and MAR-M247 in wt pct**

	Ni	Cr	Al	Mo	W	Co	Nb	Fe	Hf	Ta	C
IN 713	74 (bal.)	12	6	4	—	—	2.5	1	—	—	0.17
M247	61 (bal.)	8	5.5	0.7	10	10	0.01	0.2	1.3	3	0.16

**Table II. Sintering Parameters of Both Alloys**

Alloy	Sintering Atmosphere	Sintering Temperature (K (°C))	Holding Time (h)	Heating Rate (K/min)
IN 713	high vacuum ( $10^{-5}$ mbar)	1538 K (1265 °C)	3	10
MAR-M247	high vacuum ( $10^{-5}$ mbar)	1593 K (1320 °C)	3	10

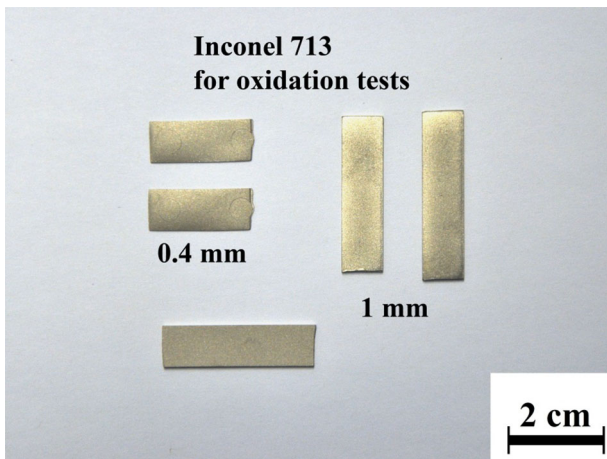


Fig. 1—MIM specimens from IN 713 for oxidation tests after sintering.

Specimens are thin platelets with a thickness of 0.4 and 1.0 mm, as shown in Figure 1. They are cut into pieces with sample length being in the range of 10 mm. The dimensions of each sample are measured individually to obtain the exact surface. The platelets are used in the “as sintered” state; neither further heat treatment nor machining is carried out afterward. Application of MIM parts in aero engines will be without any further post-processing; therefore, oxidation tests are carried out in the “as sintered” condition without any surface treatment apart from cleaning. This is in contrast to the literature data, where oxidation tests are usually reported with specimens with polished surface.<sup>[18–25]</sup> Both alloys exhibit a uniform matrix/ $\gamma'$ -microstructure with a homogeneous  $\gamma'$ -morphology in the “as sintered” state after the MIM process, see Figure 2. Due to the homogenous and favorable microstructure, both alloys are examined without further heat treatment.

For comparison and evaluation of the results of MIM-processed specimens, cast samples are tested as well. Cast samples are platelets cut from small cast parts. Cutting is in a direction that the thin side of the platelet has one untreated “as cast” surface. This side is later used for preparation of cross sections. The untreated cast surface ensures the best possible comparability with

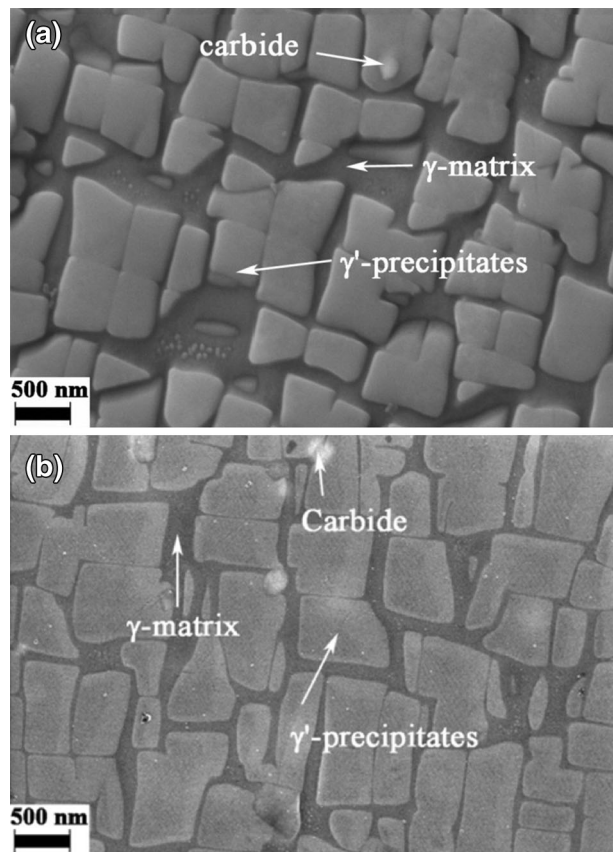


Fig. 2—(a) Microstructure of IN 713 produced by MIM in the “as sintered” state, (b) microstructure of MAR-M247 produced by MIM in the “as sintered” state.

the untreated MIM specimen surface. Both alloys exhibit uniform microstructure in the “as received” state, as shown in Figure 3. No further heat treatment on these samples was carried out as well.

Before oxidation, specimens are cleaned ultrasonically in ethanol, dried, and weighed. A balance with an accuracy of 0.01 mg is used. Oxidation experiments are carried out at temperatures from 1073 K to 1373 K (800 °C to 1100 °C) in still air with a chamber furnace Heraeus type K1252A. Specimens are standing in an  $Al_2O_3$ -holder so that the surface is in free contact with

air. An overview of the experiments is given in Table III together with the goal of each set of experiments.

In the case of IN 713, it is investigated whether the results obtained from specimens with 1.0 mm and 0.4 mm thickness differ significantly (thin-walled effect). M247 is tested after two production routes: MIM specimens are compared to cast specimens at different temperatures and times. Both types of specimens were produced according to the same material's specification. Elements' contents were checked thoroughly, including trace elements. The maximum content of sulfur (S) for both alloys was 150 ppm following the material standards for IN 713<sup>[26]</sup> and for M247, as reported by Harris *et al.*<sup>[27]</sup> In both cases, it was assured that the contents were in this range for cast and MIM material, hence

being comparable for both production routes and alloys. For each data point of MIM material shown in Table III, three samples were tested, for each of the cast material measurements, two samples were used, due to the limited amount of material.

Testing of the alloys is done discontinuously: after the times given in Table III, specimens are taken out of the oxidation furnace for analysis. They are weighed and examined by light- and scanning electron microscopy (SEM). With SEM (Zeiss EsB 1540 cross beam), the different scales and their compositions as well as the  $\gamma'$ -depletion zone are examined using different detectors and EDX. Software type Olympus AnalySIS is used to measure the thickness of oxide scales and  $\gamma'$ -depletion zone in SEM micrographs. Measurement of oxide scale thickness was carried out using between 10 and 20 micrographs for each single data point.

### III. RESULTS AND DISCUSSION

Figure 4 shows the weight gain over time at 1073 K and 1173 K (800 °C and 900 °C) for MIM samples from IN 713 with a thickness of 1.0 and 0.4 mm. Figure 5 shows the weight gain of MIM specimens after oxidation at 1273 K and 1373 K (1000 °C and 1100 °C).

One can see that the weight gain at 1073 K and 1173 K (800 °C and 900 °C) is not as regularly as one would expect from an Al<sub>2</sub>O<sub>3</sub>-controlled oxidation behavior. This indicates that other oxides control the behavior. At 1073 K (800 °C), a small weight loss is observed; a small fraction of volatile oxide is formed. At 1173 K (900 °C), the specimens exhibit a weight gain of 1 mg/cm<sup>2</sup> or less. Between the two different thicknesses, no significant differences can be observed.

Figure 5 shows that after 1273 K and 1373 K (1000 °C and 1100 °C), there is a more homogeneous weight gain for both specimen thicknesses. The weight gain at 1373 K (1100 °C) is higher than for 1273 K (1000 °C). At 1273 K (1000 °C), the thinner specimens show a higher weight gain than 1.0 mm; at 1373 K (1100 °C), thicker specimens exhibit higher weight gain. These differences are not in a range that indicates a totally different behavior depending on the thickness. Reducing the thickness from 1.0 mm to 0.4 mm is not critical for the oxidation resistance in these conditions. Therefore, further experiments in this study are all carried out with 1.0 mm specimens. Negative conse-

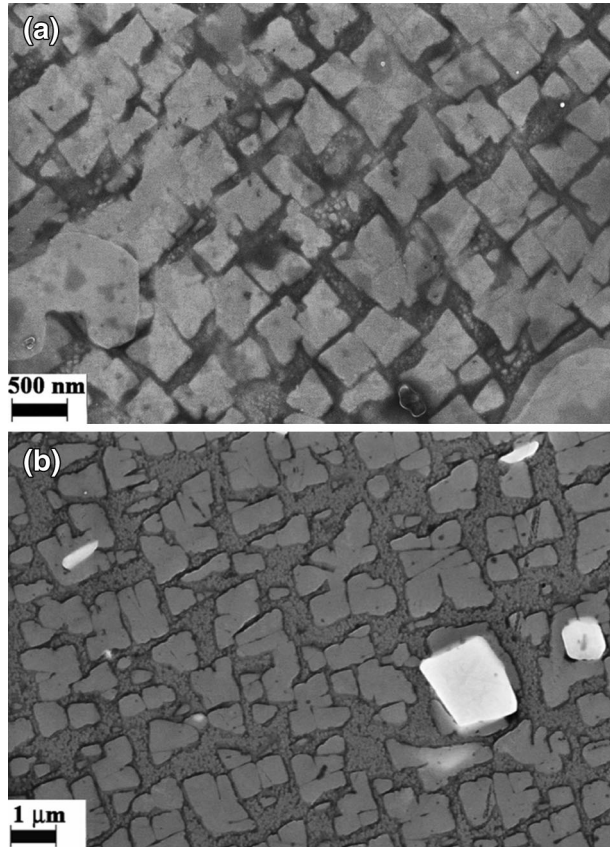


Fig. 3—(a) Microstructure of cast IN 713 in the “as received” state, (b) microstructure of cast M247 in the “as received” state.

Table III. Oxidation Experiments with Cast and MIM Samples Carried Out in Air

Alloy	Temperature (K (°C))	Oxidation Times (h)	Goal of the Experiment
IN 713	1073 K (800 °C)	100, 200, 300	comparison of specimens with a thickness of 0.4 mm and 1.0 mm
	1173 K (900 °C)		
	1273 K (1000 °C)	20, 40, 60	comparison of specimens with a thickness of 0.4 mm and 1.0 mm
	1373 K (1100 °C)		
M247	1073 K (800 °C)	100, 200, 300	comparison of MIM and cast material
	1173 K (900 °C)		
	1273 K (1000 °C)	20, 40, 60	comparison of MIM and cast material
	1373 K (1100 °C)		
	1373 K (1100 °C)	200,300	comparison of MIM and cast material
	1373 K (1100 °C)		

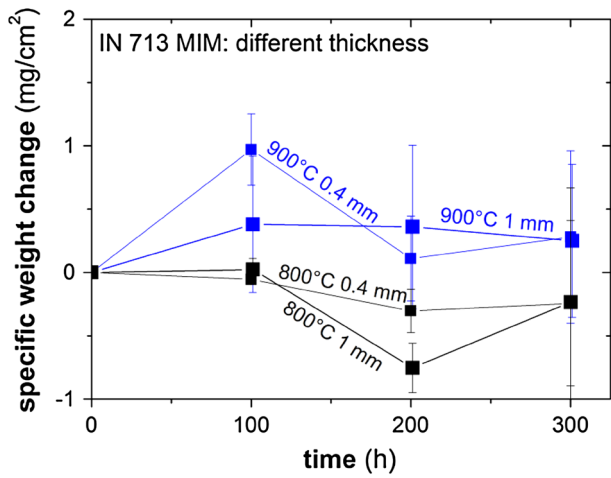


Fig. 4—Weight change of IN 713 with a specimen thickness of 0.4 and 1.0 mm after oxidation at 1073 K and 1173 K (800 °C and 900 °C).

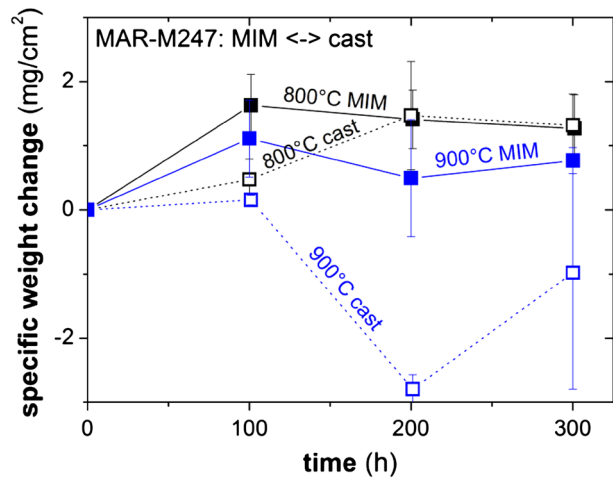


Fig. 6—Weight change of MIM and cast MAR-M247 after oxidation 1073 K and 1173 K (800 °C and 900 °C).

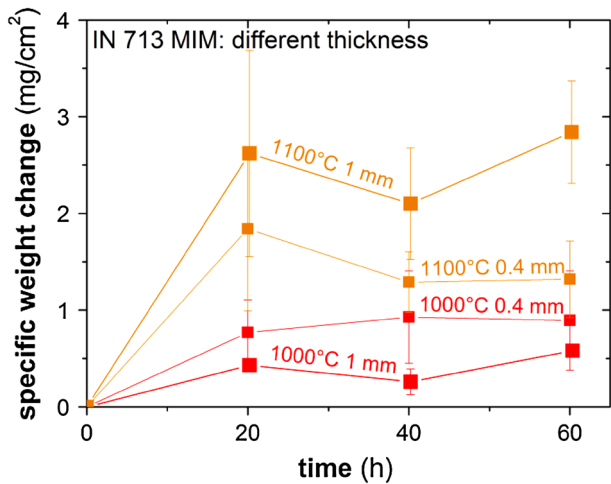


Fig. 5—Weight change of IN 713 with a specimen thickness of 0.4 and 1.0 mm after oxidation at 1273 K and 1373 K (1000 °C and 1100 °C).

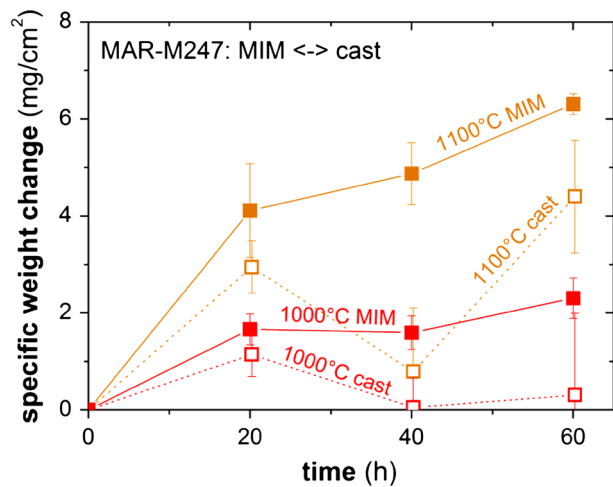


Fig. 7—Weight change of MIM and cast MAR-M247 after oxidation at 1273 K and 1373 K (1000 °C and 1100 °C).

quences of thin-walled effects for mechanical behavior like, for example, creep at high temperatures, as described by Brunner *et al.*<sup>[28]</sup> and Bensch *et al.*<sup>[29]</sup> could not be investigated in this study yet.

A comparison between cast and MIM material of MAR-M247 is given in Figures 6 and 7. At 1073 K (800 °C) (Figure 6), the weight gain of cast and MIM samples is very similar. MIM specimens exhibit weight gain for both temperatures, while cast material exhibits weight gain at 1073 K (800 °C) and a strong weight loss at 1173 K (900 °C). The oxidation behavior of MIM-processed MAR-M247 is better than that of cast MAR-M247 at 1073 K and 1173 K (800 °C and 900 °C). The raw data values of all measured weight gains are shown in Table IV. The values of IN 713 with a thickness of 1 mm after 20 and 60 hours at 1373 K (1000 °C) do not include scatter data. In these cases, two specimens had to be excluded due to a processing irregularity during weight measurement.

At 1273 K and 1373 K (1000 °C and 1100 °C) (see Figure 7), the weight gain of MIM MAR-M247 is higher than of cast MAR-M247. However, the measured weight gain is more homogeneous over time, and scatter is smaller. Tendency to spallation of cast samples is higher than of MIM samples, as illustrated by the lower weight gain at 40 hours compared to that at 20 hours as well as by the behavior at 1173 K (900 °C). This spallation causes also a lower weight gain for cast specimens in general.

Oxide layer thicknesses on both alloys after different temperatures and oxidation times are analyzed by SEM. Micrographs taken with different detectors for different information of the specimen are examined, see Figure 8. Three different outer oxide layers can be distinguished easily with the secondary electron detector, (Figure 8(a)). EDX-analyses show that the three layers are (in order from inner to outer oxide layer): Al<sub>2</sub>O<sub>3</sub>, a mixed oxide scale containing spinels, chromia, alumina, and other oxides, followed by nickel-oxide as outer oxide layer. The thickness of the outer oxide layer

**Table IV. Measured Weight Gain Data of the MIM and Cast Samples**

Temperature (K (°C))	Duration (h)	IN 713 MIM 1 mm	IN 713 MIM 0.4 mm	M247 MIM	M247 Cast
1073 K (800 °C)	100	0.02 ± 0.09	0.06 ± 0.002	1.63 ± 0.48	0.47 ± 0.32
	200	-0.75 ± 0.20	-0.30 ± 0.17	1.41 ± 0.46	1.47 ± 0.85
	300	-0.24 ± 0.90	-0.24 ± 0.65	1.27 ± 0.53	1.32 ± 0.49
1173 K (900 °C)	100	0.38 ± 0.54	0.97 ± 0.28	1.11 ± 0.60	0.15 ± 0.08
	200	0.36 ± 0.65	0.11 ± 0.34	0.49 ± 0.91	-2.80 ± 0.23
	300	0.25 ± 0.61	0.28 ± 0.68	0.77 ± 0.20	-0.98 ± 1.82
1273 K (1000 °C)	20	0.43	0.77 ± 0.34	1.66 ± 0.33	1.14 ± 0.45
	40	0.26 ± 0.13	0.93 ± 0.48	1.59 ± 0.23	0.05 ± 0.60
	60	0.58	0.89 ± 0.51	2.31 ± 0.42	0.31 ± 1.69
1373 K (1100 °C)	20	2.62 ± 1.07	1.84 ± 0.85	4.11 ± 0.97	2.95 ± 0.54
	40	2.10 ± 0.58	1.29 ± 0.31	4.87 ± 0.64	0.79 ± 1.31
	60	2.84 ± 0.53	1.32 ± 0.40	6.31 ± 0.22	4.40 ± 1.16

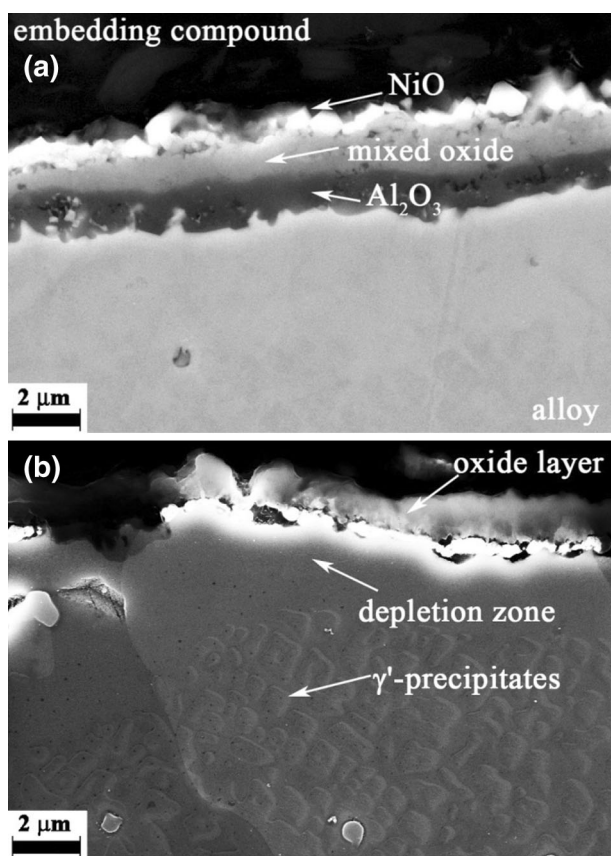


Fig. 8—(a) Secondary electron image of IN 713 MIM after oxidation at 1273 K (1000 °C) for 40 h with three distinctive oxide layers, (b) In-Lens-micrograph of IN 713 MIM after oxidation at 1173 K (900 °C) for 100 h with visible depletion of  $\gamma'$  beneath the oxide layers.

consisting of NiO was not considered for thickness measurements, since this oxide tends to extensive spallation. InLens-micrographs show the depletion of  $\gamma'$ -precipitates underneath the oxide layers, because Al from the  $\text{Ni}_3\text{Al}$ -precipitates diffuses to the surface during the formation of  $\text{Al}_2\text{O}_3$ , (Figure 8(b)), as it is explained, for example, by Gesmundo and Gleeson.<sup>[30]</sup> A modeling approach of these phenomena for two

$\text{Al}_2\text{O}_3$ -forming commercial superalloys can be found as well.<sup>[31]</sup>

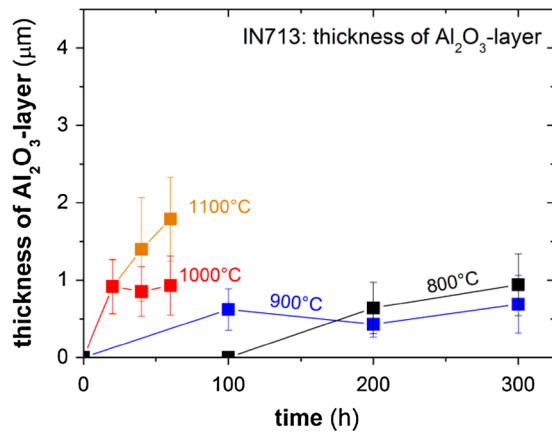
The measured thickness of the oxide layers for both alloys processed by MIM is shown in Figure 9. The layer thicknesses of IN 713 are shown in Figures 9(a), (c), (e), the thicknesses of MAR-M247 are shown in Figures 9(b), (d), (f). The corresponding values to these figures are listed in Tables V and VI.

At 1073 K (800 °C), the formation of a continuous  $\text{Al}_2\text{O}_3$  layer on both alloys can only be observed after fairly long oxidation times, in case of IN 713 after times longer than 100 hours. A homogeneous  $\text{Al}_2\text{O}_3$  layer is formed at 200 and 300 hours, as Figure 10 shows. Despite this, a small depletion zone is visible already at 100 hours.

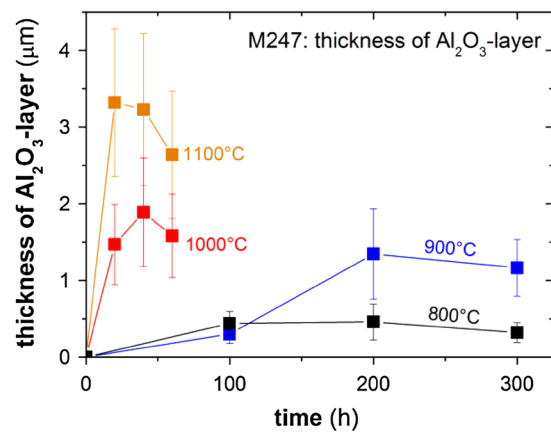
MAR-M247 builds a thin, not entirely continuous layer of  $\text{Al}_2\text{O}_3$  after 100 hours at 1073 K (800 °C). The oxidation behavior is controlled by the formation of a fast-growing layer of mixed oxide. At longer oxidation times than 200 hours, this rather thick layer starts to spall off. The weight gain in Figure 6 as well as the layer thickness in Figure 9(d) both demonstrate this behavior. Both measurements obtain a maximum at 100 hours with higher weight gain and layer thickness than after oxidation at 1173 K (900 °C). At 300 hours, a high fraction of this mixed oxide has spalled, and the  $\text{Al}_2\text{O}_3$ -layer is continuous. A small depletion zone has formed as well, see Figure 9(f). At higher temperatures, the formation of  $\text{Al}_2\text{O}_3$  is faster, so these observations are not made at 1173 K to 1373 K (900 °C to 1100 °C). For use in operation at 1073 K (800 °C), preoxidation at higher temperatures is a possibility to enhance a fast formation of  $\text{Al}_2\text{O}_3$ .

IN 713 shows especially at 1273 K and 1373 K (1000 °C and 1100 °C) homogeneous, slow growing oxide layers with a thickness  $< 2 \mu\text{m}$  (Figures 9(a), (c)). Oxide layers on MAR-M247 are thicker with a thickness up to  $4 \mu\text{m}$  at 1373 K (1100 °C) (Figures 9(b), (d)). Thickness is constant in the interval from 20 to 60 hours. At all tested conditions, MIM samples exhibit thin continuous oxide layers.

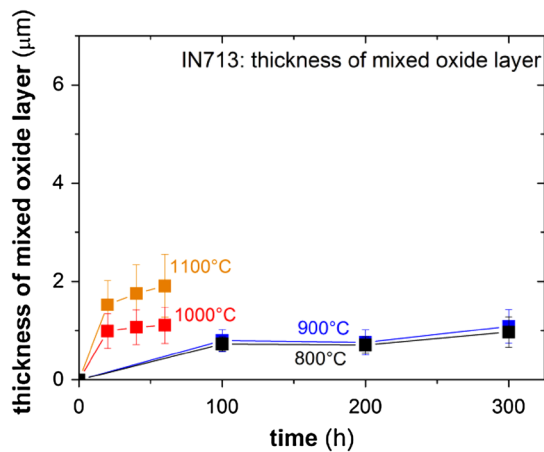
The morphology and the microstructure of the  $\text{Al}_2\text{O}_3$  layer can be seen in SEM using the InLens detector, see Figure 11. Grains inside the oxide layer are visible.



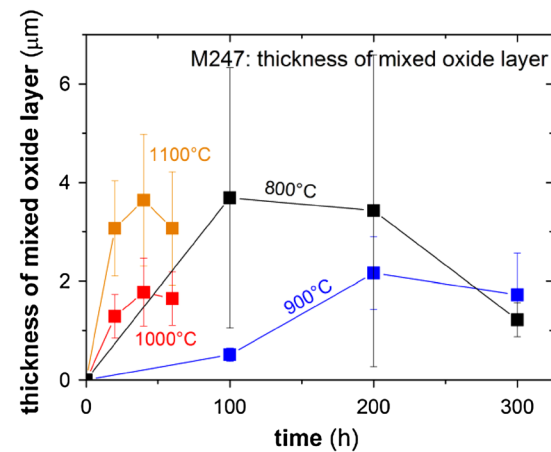
(a) Al<sub>2</sub>O<sub>3</sub>-layer on IN 713



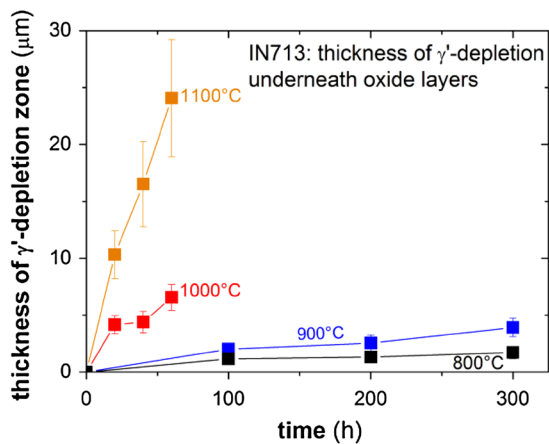
(b) Al<sub>2</sub>O<sub>3</sub>-layer on M247



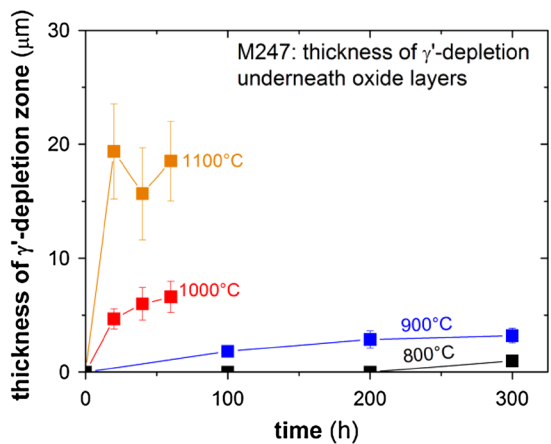
(c) mixed oxide layer on IN 713



(d) mixed oxide layer on M247



(e) depletion zone in IN 713



(f) depletion zone in M247

Fig. 9—Thickness of oxide layers of MIM-processed alloys IN 713 and MAR-M247 with specimen thickness of 1.0 mm after oxidation at (1073 K to 1373 K (800 °C to 1100 °C)).

The Al<sub>2</sub>O<sub>3</sub> layer consists of small grains that are mostly equiaxial. This is an indication that no reactive elements like Yttrium, which would favor a columnar grain growth,<sup>[32]</sup> are present in the layer. The grain

boundaries are diffusion paths for ions through the oxide layer. With this, further investigations of formation, growth, and properties of the oxide layer are possible.

**Table V. Layer Thickness Data of IN 713 MIM**

Temperature (K (°C))	Duration (h)	Mixed Oxide ( $\mu\text{m}$ )	$\text{Al}_2\text{O}_3$ ( $\mu\text{m}$ )	Depletion Zone ( $\mu\text{m}$ )
1073 K (800 °C)	100	$0.73 \pm 0.14$	0	$1.15 \pm 0.22$
	200	$0.71 \pm 0.17$	$0.64 \pm 0.17$	$1.31 \pm 0.44$
	300	$0.97 \pm 0.31$	$0.94 \pm 0.40$	$1.71 \pm 0.54$
1173 K (900 °C)	100	$0.80 \pm 0.22$	$0.62 \pm 0.27$	$2.01 \pm 0.40$
	200	$0.76 \pm 0.26$	$0.43 \pm 0.17$	$2.54 \pm 0.72$
	300	$1.09 \pm 0.34$	$0.69 \pm 0.37$	$3.92 \pm 0.81$
1273 K (1000 °C)	20	$0.99 \pm 0.35$	$0.92 \pm 0.35$	$4.16 \pm 0.80$
	40	$1.07 \pm 0.35$	$0.85 \pm 0.32$	$4.39 \pm 0.94$
	60	$1.11 \pm 0.37$	$0.93 \pm 0.38$	$6.56 \pm 1.12$
1373 K (1100 °C)	20	$1.53 \pm 0.49$	$0.91 \pm 0.35$	$10.32 \pm 2.11$
	40	$1.76 \pm 0.58$	$1.40 \pm 0.67$	$16.53 \pm 3.75$
	60	$1.91 \pm 0.64$	$1.79 \pm 0.54$	$24.08 \pm 5.16$

**Table VI. Layer Thickness Data of MAR-M247 MIM**

Temperature (K (°C))	Duration (h)	Mixed Oxide ( $\mu\text{m}$ )	$\text{Al}_2\text{O}_3$ ( $\mu\text{m}$ )	Depletion Zone ( $\mu\text{m}$ )
1073 K (800 °C)	100	$3.69 \pm 2.64$	$0.44 \pm 0.16$	—
	200	$3.43 \pm 3.16$	$0.46 \pm 0.24$	—
	300	$1.22 \pm 0.34$	$0.32 \pm .013$	$0.98 \pm 0.27$
1173 K (900 °C)	100	$0.51 \pm 0.14$	$0.30 \pm 0.12$	$1.83 \pm 0.52$
	200	$2.16 \pm 0.74$	$1.35 \pm 0.59$	$2.86 \pm 0.75$
	300	$1.72 \pm 0.84$	$1.16 \pm 0.37$	$3.20 \pm 0.63$
1273 K (1000 °C)	20	$1.29 \pm 0.44$	$1.47 \pm 0.52$	$4.67 \pm 0.89$
	40	$1.78 \pm 0.68$	$1.89 \pm 0.71$	$5.98 \pm 1.43$
	60	$1.65 \pm 0.54$	$1.58 \pm 0.54$	$6.60 \pm 1.38$
1373 K (1100 °C)	20	$3.07 \pm 0.96$	$3.32 \pm 0.96$	$19.37 \pm 4.16$
	40	$3.64 \pm 1.34$	$3.23 \pm 0.99$	$15.66 \pm 4.04$
	60	$3.07 \pm 1.15$	$2.64 \pm 0.83$	$18.53 \pm 3.50$

Weight gain as well as layer thicknesses show that the oxidation behavior at temperatures above 1073 K (800 °C) is controlled by  $\text{Al}_2\text{O}_3$ . Weight gain can be described by a parabolic growth law and a constant  $k_p$ , see Eq. [1].

$$k_p = 1/t (\Delta m/A)^2 \quad [1]$$

The different parabolic constants for oxidation at 1173 K to 1373 K (900 °C to 1100 °C) for MIM alloys IN 713 and MAR-M247 are shown in Table VII. The given constants are derived from the measuring point at different times, therefore, being average values for the respective temperatures. The average values lie within the scatter band of the single data points, despite the occurrence of spalling.

The parabolic time constants for both alloys increase by one order of magnitude if the temperature is increased by 100 K (−173 °C). IN 713 exhibits a value of  $k_p$  that is one order of magnitude lower than that of MAR-M247.

Temperature dependence for both alloys and temperatures of 1173 K, 1273 K, and 1373 K (900 °C, 1000 °C and 1100 °C) is shown in an Arrhenius plot in Figure 12. The activation energies calculated from the slope of  $\ln(k_p)$  vs  $1/T$  are  $Q_{\text{IN713}} = 368$  kJ/mol and  $Q_{\text{M247}} = 322$  kJ/mol.

Weight gain data of cast IN 713 have been described in the literature.<sup>[19–22,25]</sup> Fryburg *et al.*<sup>[25]</sup> determine a parabolic constant  $k_p$  of  $3.53 \times 10^{-10}$   $\text{kg}^2 \text{m}^{-4} \text{s}^{-1}$  during oxidation for 2 to 50 hours at 1173 K (900 °C), albeit in flowing oxygen, not air. This is one order of magnitude higher than the value of  $k_p$  for IN 713 processed by MIM.

The weight gain of cast IN 713 reported by Christ *et al.*<sup>[19]</sup> for oxidation at 1123 K (850 °C) up to 300 hours and 1273 K (1000 °C) up to 100 hours is in the range of 0.3 to 0.4  $\text{mg}/\text{cm}^2$ , which is comparable to the weight gain of the MIM-processed material in this study. Barrett *et al.*<sup>[20]</sup> and Mahapatra *et al.*<sup>[21,22]</sup> report weight gain in a similar range for cast IN 713 at 1273 K (1000 °C). The literature data for oxidation at 1373 K (1100 °C) are lower than the values obtained in this study. MIM-processed material exhibits a weight gain in the range of 2.5  $\text{mg}/\text{cm}^2$ , while cast material is in the range of 1.5  $\text{mg}/\text{cm}^2$ .<sup>[21]</sup>

Weight gain of cast alloy CM247 LC is described by Das *et al.*<sup>[18]</sup> at 1373 K (1100 °C). This alloy has been developed on the base of MAR-M247 and has a very similar composition. The reported weight gain of CM247 LC is higher than that of MIM-processed MAR-M247. CM247 LC exhibits parabolic oxidation behavior after 20 hours. Weight gain between 20 and 100 hours is in the range from 6 to 9  $\text{mg}/\text{cm}^2$ . MIM-processed MAR-M247 in this study exhibits a weight

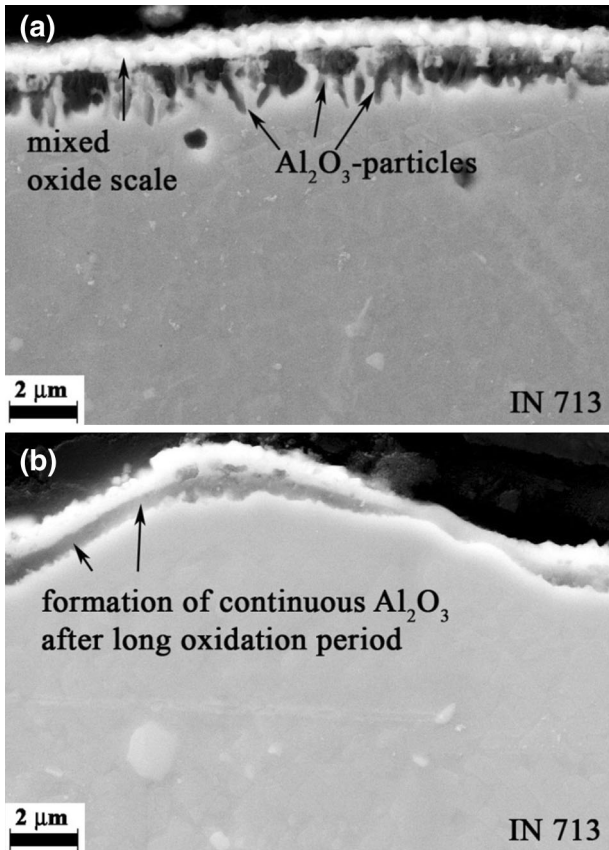


Fig. 10—(a) SEM micrograph of  $\text{Al}_2\text{O}_3$  on IN 713 after oxidation at 1073 K (800 °C) for 100 h, (b) SEM micrograph of IN 713 after oxidation at 1073 K (800 °C) for 300 h.

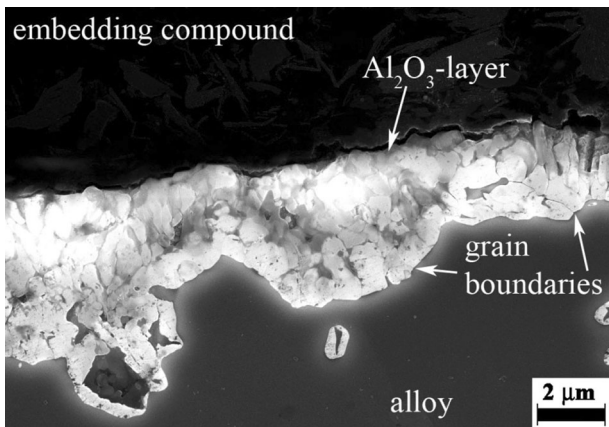


Fig. 11—SEM micrograph of  $\text{Al}_2\text{O}_3$ -grain structure on IN 713, after 1373 K (1100 °C) for 60 h.

gain from 4 to 6  $\text{mg}/\text{cm}^2$  at 20 to 60 hours at 1373 K (1100 °C).

In contrast to MIM-processed material, oxidized cast specimens in this study do not form homogeneous and distinctive oxide layers. Figure 13 shows the comparison of an oxidized MIM (Figure 13(a)) and a cast sample (Figure 13(b)) of MAR-M247 after oxidation at 1373 K

Table VII. Parabolic Oxidation Constants  $k_p$  in  $\text{kg}^2 \text{m}^{-4} \text{s}^{-1}$  for MIM Alloys After Oxidation at 1173 K to 1373 K (900 °C to 1100 °C)

Alloy	$k_p$ at 1173 K (900 °C)	$k_p$ at 1273 K (1000 °C)	$k_p$ at 1373 K (1100 °C)
IN 713	$2.12 \times 10^{-11}$	$1.66 \times 10^{-10}$	$5.46 \times 10^{-9}$
MAR-M247	$1.44 \times 10^{-10}$	$2.69 \times 10^{-9}$	$1.95 \times 10^{-8}$

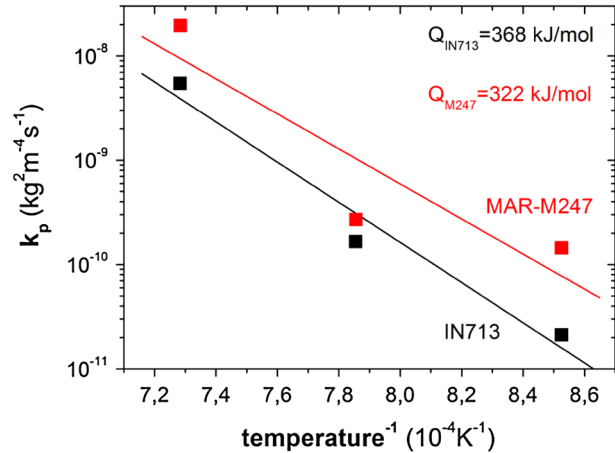


Fig. 12—Arrhenius plot for  $k_p$  for MIM-processed alloys IN 713 and MAR-M247.

(1100 °C) and 40 hours. The MIM-processed surface shows homogeneous, uniform oxide layers, while the untreated cast surface exhibits inhomogeneous oxide layer thickness. The oxide grows further inward in case of the cast surface. A comparison of oxide layer thickness on MIM and cast samples is not reasonable. Therefore, the thickness of the depletion zone of MIM and cast specimens is compared. This gives a measurement how much material inside the sample is directly affected by oxidation. If the depletion zone gets too thick, the diffusion length for Al to diffuse to the surface to form  $\text{Al}_2\text{O}_3$  increases. After long oxidation periods, the protective oxide layer cannot be formed anymore, and the alloy fails. Inherently, without  $\gamma'$ -precipitates in the outer region of the sample, the alloy loses high temperature and creep strength.

Comparison of depletion zone thickness after 1173 K and 1273 K (900 °C and 1000 °C) for both alloys is shown in Figure 14. After 1173 K (900 °C), the thickness of the  $\gamma'$ -depletion in cast samples is higher than in MIM samples (Figure 14(a)). There is no significant difference observed in oxidation behavior between the two alloys. MIM-processed material exhibits a similar thickness of depletion of 2 to 3  $\mu\text{m}$ ; the thickness of the depletion zone in both cast alloys is 4 to 5  $\mu\text{m}$ . After 1273 K (1000 °C), the differences for all tested samples are very low, and the thickness of  $\gamma'$ -depletion is around 4 to 6  $\mu\text{m}$  (Figure 14(b)). One exception is cast IN 713, where the depletion zone after 60 hours shows a thickness of 12  $\mu\text{m}$ . The literature data of cast IN 713<sup>[20]</sup> show a thicker  $\gamma'$ -depletion zone than observed in this study.



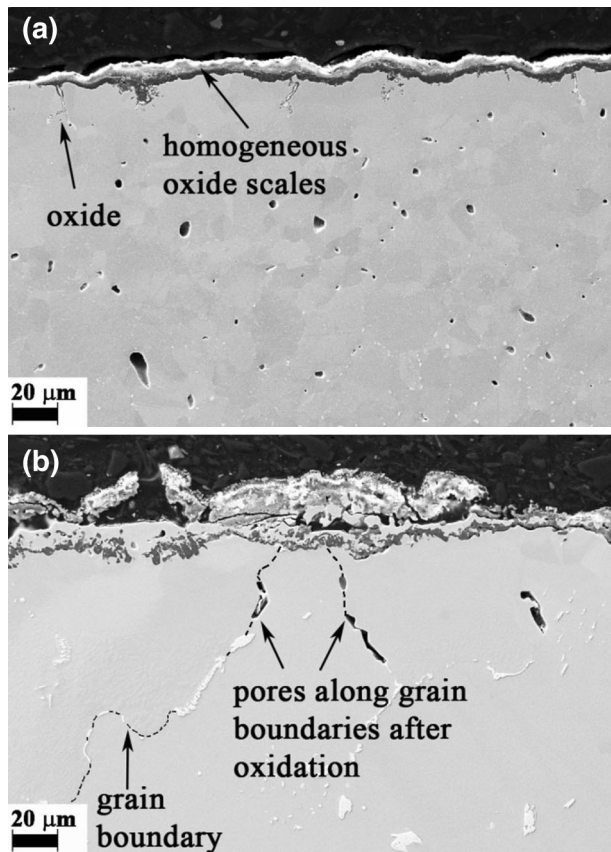


Fig. 13—(a) MIM-processed MAR-M247 with homogeneous oxide scales after 40 h at 1373 K (1100°C), (b) Cast MAR-M247 after oxidation at 1373 K (1100 °C) for 40 h without homogeneous oxide scales and higher oxidation attack inside the sample.

A comparison of  $\gamma'$ -depletion zone of MIM and cast material after oxidation at 1373 K (1100 °C) is not possible with the results of this study. Barrett reports a depletion zone in cast IN 713 after 1373 K (1100 °C) with a thickness of over 50  $\mu\text{m}$ .<sup>[20]</sup>

The oxidation resistance of MAR-M247 at 1373 K (1100 °C) after 200 and 300 hours is tested for MIM and cast specimens. This temperature exceeds the usual operation temperatures for MAR-M247. SEM micrographs after 200 hours at 1373 K (1100 °C) are shown in Figure 15. On the MIM-processed alloy, very thick oxide layers with a thickness up to 50 to 100  $\mu\text{m}$  have formed. These oxides grow partially inward, see Figure 15(a). However, a thin oxide layer is found on the surface at sites, where thick layers already have spalled off. The cast specimen does not exhibit these thick oxide scales (Figure 15(b)). Traces can be found in the specimens' holder that the oxide layers already have spalled off. No oxide layer is found on the surface of the sample. Oxide particles after internal oxidation within the specimen are observed. Without the protective oxide layer, oxides grow fast internally and thereby increase the oxidation attack.

After 300 hours at 1373 K (1100 °C), a significant difference between MIM and cast samples is observed, see Figure 16. MIM samples show a homogeneous oxide layer and are still intact (Figure 16(a)). In contrast, the

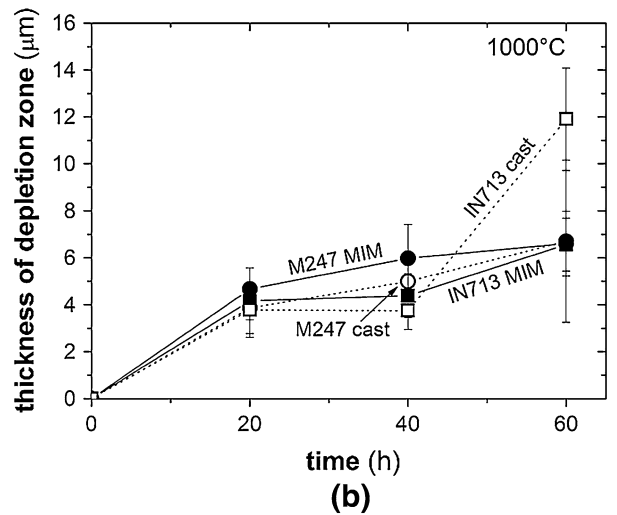
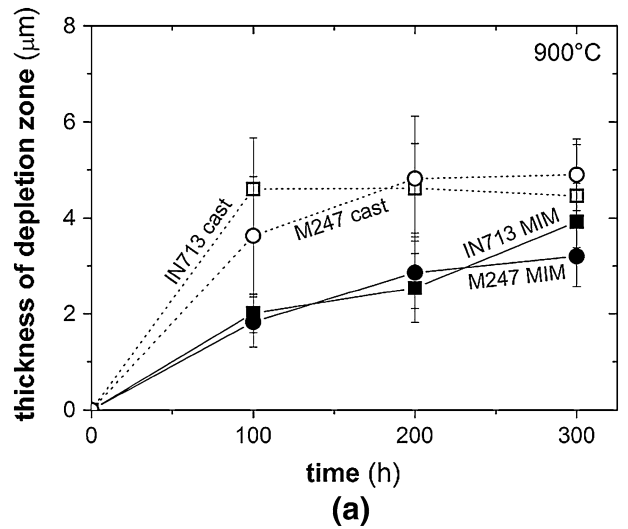


Fig. 14—(a) Measured thickness of depletion zone in MIM and cast specimens from IN 713 and MAR-M247 after oxidation at 1173 K (900 °C), (b) measured thickness of  $\gamma'$  depletion zone in IN 713 and MAR-M247 for two processing routes after oxidation at 1273 K (1000 °C).

cast samples are completely oxidized, and catastrophic failure without mechanical load has occurred (Figure 16(b)). The upper part of the samples is free from oxide layers due to spallation. At these oxidation and surface preparation conditions, MIM samples show an advantage in oxidation resistance.

The explanation for this observation can be given by the microstructure after the different processing routes. MIM-processed samples in this study exhibit a fine-grained microstructure with a grain size in-between 10 and 20  $\mu\text{m}$ . The grains in the cast alloys are much coarser with grain size >100  $\mu\text{m}$ . The oxidation front follows grain boundaries. Oxidation effects at the grain boundaries are shown in Figure 13. Especially for the cast sample in Figure 13(b), pores at the grain boundary after oxidation are observed.

Oxidized grain boundaries in MIM-processed samples are much shorter, until they have to spread out at triple boundaries, so there is no direct diffusion path deeper

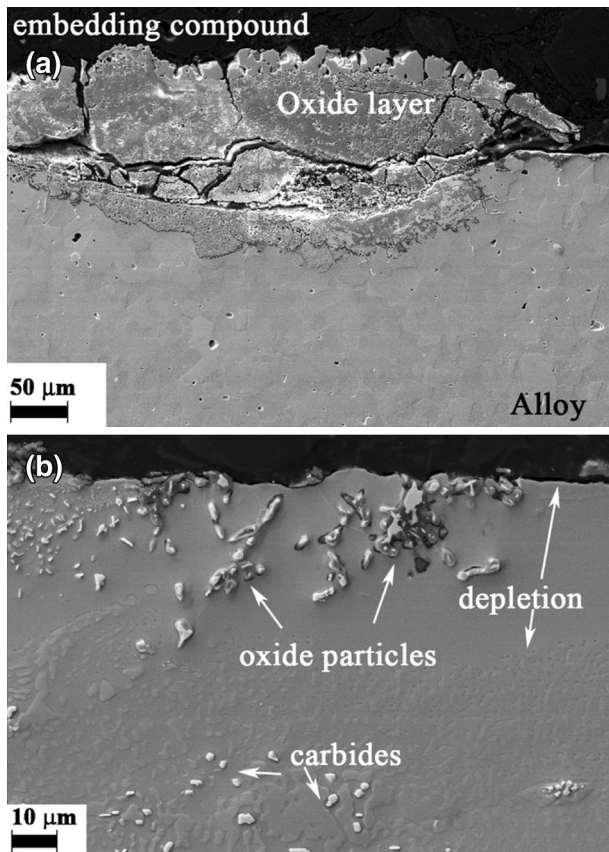


Fig. 15—(a) SEM micrograph of MIM MAR-M247 after oxidation for 200 h at 1373 K (1100 °C), (b) SEM micrograph of cast MAR-M247 after oxidation for 200 h at 1373 K (1100 °C).

inside the sample. On the other hand, grain boundaries in cast samples go more or less perpendicular from the surface into the sample. Thus, a more direct diffusion path for oxygen is given. Another advantage of the MIM-processing route is the more homogeneous microstructure. Since there are no casting defects like segregation, eutectics, or dendritic structure, the chemistry of the grain boundary in the MIM alloys is more homogeneous and with that more resistant against oxidation attack.

Further steps to a complete understanding of the grain boundaries' role in oxidation resistance in a MIM-processed alloy will include a closer look at varying trace elements' contents. Since the samples in this study show a considerable amount of spallation, further investigations concerning the role of S in these specimens need to be conducted, including a comparison of distribution between MIM and cast samples concerning segregation and other effects also using extensive literature data.<sup>[33–38]</sup> One step hereby is an examination of MIM-produced parts from CM-247 LC which has a significant lower maximum S level of 15 ppm<sup>[27]</sup> in comparison with a conventionally cast M247.

Further investigations are to get a deeper insight on the role of phases like  $\gamma'$ , carbides, and carbonitrides.

Another point that can be looked at in further experiments is a comparison of polished samples of

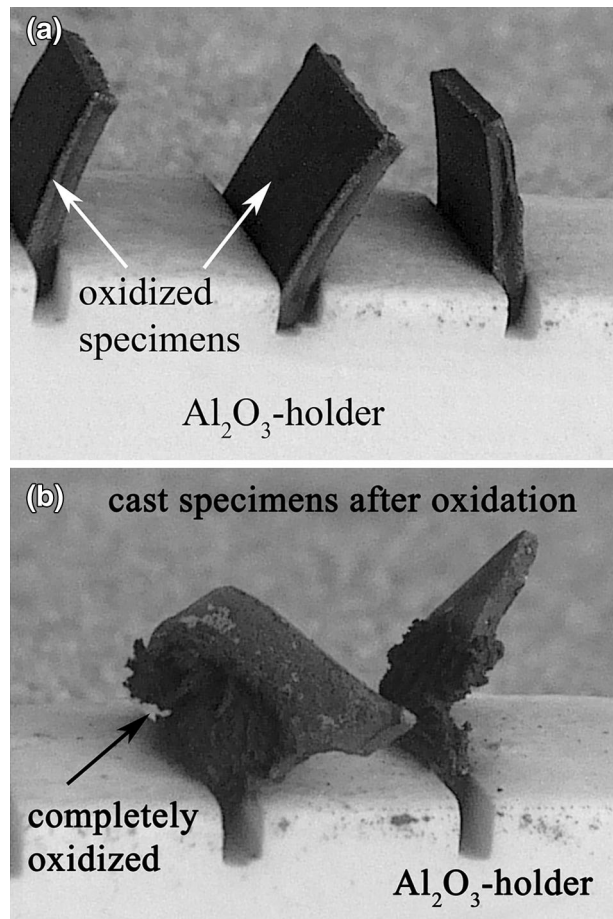


Fig. 16—(a) MIM samples of MAR-M247 after oxidation at 1373 K (1100 °C) for 300 h, bending due to sintering step, not due to oxidation, (b) cast samples of MAR-M247 after oxidation at 1373 K (1100 °C) for 300 h.

MIM-processed and cast alloys to diminish the scatter and surface effects. This is a step away from the application-based investigations in this study but again a little further into detail.

#### IV. CONCLUSIONS

Oxidation behavior of nickel based-superalloys IN 713 and MAR-M247 produced by metal injection molding is investigated in the temperature range of 1073 K to 1373 K (800 °C to 1100 °C) in order to evaluate the potential of this process for high-temperature applications. Both alloys exhibit thin, homogeneous oxide layers with three different layers.  $\text{Al}_2\text{O}_3$ , a mixed oxide consisting of spinel, chromia, and smaller fractions of other oxides, and a NiO-layer that tends to spall off easily. Layer thickness of individual oxide layers on MIM-produced IN 713 is up to 2 μm, while the layers on MAR-M247 exhibit a thickness up to 4 μm. While both MIM alloys exhibit homogeneous oxide layers, cast alloys IN 713 and MAR-M247 form oxide layers with more varying thickness and morphology.

The main conclusions are:

1. At 1073 K (800 °C), formation of a dense Al<sub>2</sub>O<sub>3</sub> layer on MIM alloys is not completed, until oxidation times up to 100 hours in case of IN 713 and 200 hours in case of MAR-M247. Up to this point, oxidation behavior is controlled by a fast-growing mixed oxide layer, which spalls after further oxidation. At this temperature, preoxidation is a possibility to enhance the formation of Al<sub>2</sub>O<sub>3</sub>.
2. At 1173 K to 1373 K (900 °C to 1100 °C), oxidation of both MIM alloys is controlled by Al<sub>2</sub>O<sub>3</sub>. Weight gain can be described by a parabolic oxidation constant,  $k_p$  and a correspondent activation energy  $Q$ . This constant increases by one order of magnitude, if the temperature is increased by 100 K. IN 713 exhibits a parabolic time constant one order of magnitude lower than MAR-M247. Weight gain of both alloys is better or in the same range as the literature data.
3. Up to 1373 K (1100 °C) for 60 hours and 0.4 mm thin samples, a thin-walled effect on oxidation of MIM-processed specimens could not be observed.
4. For both alloys, advantages in oxidation resistance of the MIM-processed surface can be explained by the finer grain size of MIM samples (10 to 20 μm) as compared to cast samples (>100 μm).
5. IN 713 and MAR-M247 produced by MIM show good potential for operation in oxidizing conditions with advantages of IN 713 over MAR-M247.

#### ACKNOWLEDGMENTS

The authors thank Bundesministerium für Wirtschaft und Technologie (BMWi) for funding as well as MTU Aero Engines and Schunk Sintermetalltechnik for research cooperation via the LuFo IV/2 research program.

#### REFERENCES

1. R.M. German and A. Bose: *Injection Molding of Metals and Ceramics*, MPIF, Princeton, NJ, 1997.
2. R.M. German: *Metal Injection Molding, A Comprehensive MIM Design Guide*, MPIF, Princeton, NJ, 2011.
3. H. Wohlfromm, A. Ribbens, J. ter Maat, and M. Blömacher: *Proc. Euro PM*, 2003, vol. 2003, pp. 207–15.
4. A. Kern, M. Blömacher, J. ter Maat, and A. Thom: *Met. Powder Rep.*, 2011, vol. 66, pp. 22–26.
5. A. Bose, J.J. Valencia, J. Spirko, and R. Schmees: *Adv. Powder Metal. Part. Mater.*, 1997, vol. 3, pp. 18.99–18.112.
6. J.J. Valencia, T. McCabe, K. Hens, J.O. Hansen, and A. Bose: in *Superalloys 718, 625, 706 and various Derivatives*, E.A. Loria, ed., TMS, Warrendale, PA, 1994, pp. 935–45.
7. E. Lange and M. Poniakowski: *Z. Werkst.*, 1987, vol. 18, pp. 337–44.
8. B.N. Nobrega, W. Ristow, Jr., and R. Machado: *Powder Met.*, 2008, vol. 51, pp. 107–10.
9. P.A. Davies, G.R. Dunstan, R.I.L. Howells, and A.C. Hayward: *Met. Powder Rep.*, 2004, vol. 59, pp. 14–19.
10. W. Diehl, H. Buchkremer, H. Kaiser, and D. Stöver: *Werkst. Innov.*, 1988, vol. 1, pp. 48–51.
11. B. Klöden, U. Jehring, T. Weißgärber, and B. Kieback: *Proc. World PM 2010*, Florence, 2010, vol. 4, pp. 413–20.
12. E.A. Ott and M.W. Peretti: *JOM*, 2012, vol. 64, pp. 252–56.
13. N. Salk: *PIM Int.*, 2011, vol. 5, pp. 61–64.
14. H. Miura, H. Ikeda, T. Iwahashi, and T. Osada: *PIM Int.*, 2010, vol. 4, pp. 68–70.
15. J.L. Smialek and G.H. Meier: in *Superalloys II: High-Temperature Materials for Aerospace and Industrial Power*, C.T. Sims, N.S. Stoloff, and W.C. Hagel, eds., Wiley, New York, 1987, pp. 293–325.
16. C.S. Giggins and F.S. Pettit: *J. Electrochem. Soc.*, 1971, vol. 118, pp. 1782–90.
17. C. Wagner: *J. Electrochem. Soc.*, 1956, vol. 103, pp. 627–33.
18. D.K. Das, V. Singh, and S.V. Joshi: *Mater. Sci. Technol.*, 2003, vol. 19, pp. 695–707.
19. H.J. Christ, L. Berchthold, and H.G. Sockel: *Oxid. Met.*, 1986, vol. 26, pp. 45–76.
20. C.A. Barrett, G.J. Santoro, and C.E. Lowell: “Isothermal and Cyclic Oxidation at 1000 °C and 1100 °C of Four Nickel-base alloys: NASA-TRW VIA, B-1900, 713C, and 738X”, NASA Technical Note, TN D-7484, 1973.
21. R.N. Mahapatra, S.K. Varma, C. Lei, and V.V. Agarwala: *Oxid. Met.*, 2004, vol. 62, pp. 93–102.
22. R.N. Mahapatra, S.K. Varma, and C.S. Lei: *Oxid. Met.*, 2006, vol. 66, pp. 127–135.
23. H. Wei, G.C. Hou, X.F. Sun, H.R. Guan, and Z.Q. Hu: *Oxid. Met.*, 2007, vol. 68, pp. 149–63.
24. X.J. Zhang, S.Y. Wang, F. Gesmundo, and Y. Niu: *Oxid. Met.*, 2006, vol. 65, pp. 151–65.
25. G.C. Fryburg, F.J. Kohl, and C.A. Stearns: “Oxidation in Oxygen at 900 °C and 1000 °C of four Nickel-Base Cast Superalloys: Nasa-TRW VIA, B-1900, Alloy 713C, and IN-738”, NASA Technical Note, TN D-8388, 1977.
26. German Material Specification WL 2.4671, Beuth, Berlin, 1984.
27. K. Harris, G.L. Erickson, and R.E. Schwer: *Proc. Fifth Int. Symp. Superalloys*, Metallurgical Society AIME, Warrendale, PA, 1984, pp. 221–30.
28. M. Brunner, M. Bensch, R. Völkl, E. Affeldt, and U. Glatzel: *Mater. Sci. Eng. A*, 2012, vol. 550, pp. 254–62.
29. M. Bensch, J. Preußner, R. Hüttner, G. Obigodi, S. Virtanen, J. Gabel, and U. Glatzel: *Acta Mater.*, 2010, vol. 58, pp. 1607–17.
30. F. Gesmundo and B. Gleeson: *Oxid. Met.*, 1995, vol. 44, pp. 211–37.
31. M. Bensch, A. Sato, N. Warnken, E. Affeldt, R.C. Reed, and U. Glatzel: *Acta Mater.*, 2012, vol. 60, pp. 5468–80.
32. F.H. Stott, G.C. Wood, and J. Stringer: *Oxid. Met.*, 1995, vol. 44, pp. 113–45.
33. M.A. Smith, W.E. Frazier, and B.A. Pregar: *Mater. Sci. Eng. A*, 1995, vol. 203, pp. 388–98.
34. J.G. Smeggil, A.W. Funkenbush, and N.S. Bornstein: *Metall. Trans. A*, 1986, vol. 17, pp. 923–32.
35. J.G. Smeggil, N.S. Bornstein, and M.A. DeCrescente: *Oxid. Met.*, 1988, vol. 30, pp. 259–66.
36. P.Y. Hou and J. Stringer: *Oxid. Met.*, 1992, vol. 38, pp. 323–45.
37. D.G. Lees: *Oxid. Met.*, 1987, vol. 27, pp. 75–81.
38. J.L. Smialek: *Metall. Trans. A*, 1991, vol. 22, pp. 739–52.